Journal of Thermal Science

https://doi.org/10.1007/s11630-020-1324-0

Modeling De-NO_x by Injection Ammonia in High Temperature Zone of Cement Precalciner

ZHANG Leyu[1,3], WEI Xiaolin[1,2*], ZHANG Zhongxiao[3*], LI Sen[1]

1. Institute of Mechanics, Chinese Academy of Sciences, Beijing 100190, China
2. School of Engineering Science, University of Chinese Academy of Sciences, Beijing 100190, China
3. School of Environment and Architecture, University of Shanghai for Science and Technology, Shanghai 200093, China

Abstract: The quantity of NO_x emission from cement production is second only to thermal power generation and vehicle exhaust. In this paper, a phenomenon found by Taniguchi is used to achieve NO_x reduction in the cement precalciner. Based on his results, it is proposed to reduce NO_x that ammonia is injected in the high-temperature and lean-oxygen zone (HT-DeNO_x) during pulverized coal combustion. For a large cement precalciner (3200 t/d), numerical simulation is used to evaluate the technology of HT-DeNO_x combined with the traditional selective non-catalytic reduction (SNCR) method. The results indicate that NH_3 and HCN in HT-DeNO_x can reduce NO during the reaction process. With very little ammonia injection (normalized stoichiometric ratio NSR=0.1, the normalized stoichiometric ratio), the efficiency of NO reduction by HT-DeNO_x is 27.72%. Combining SNCR (NSR=1.1) and HT-DeNO_x (NSR=0.1), the reduction efficiency will be improved to 60.05%, compared with 50.83% efficiency when using only SNCR at NSR=1.2.

Keywords: cement precalciner, coal combustion, $CaCO_3$ decomposition, high temperature zone, SNCR

1. Introduction

The precalciner is one of the most important pieces of equipment in the cement production process, serving as a container for both pulverized coal combustion and raw material decomposition reactions. Its temperature range is approximately 870°C to 1050°C, and the selective non-catalytic reduction (SNCR) method is suitable for NO_x removal, or De-NO_x, in the precalciner. High CO_2 and CaO concentrations in the precalciner make its internal environment significantly different from the utility boiler, as shown in Table 1. Therefore, it is very important to select the ammonia injection position, which is closely related to the flow field, temperature distribution, gas phase residence time, and material distribution in the precalciner [1].

Table 1 The comparison of gas composition and temperature between utility boiler and precalciner [2–5]

Type	Utility boiler	Precalciner kilns system
CO_2 concentration	About 15%	15% to 30%
CaO concentration	Negligible	1 kg(CaO)/m^3(flue gas)
Temperature/°C	1200 to 1600	870 to 1050
OFA temperature/°C	20 to 200	About 900

Received: Jul 11, 2019
AE: YANG Bin

Corresponding author: WEI xiaolin
ZHANG zhongxiao

E-mail: xlwei@imech.ac.cn
zhzhx222@163.com

Li [6] and Liu [7] both employed computational fluid dynamics (CFD) to study the flow field distribution of cyclone separators and the gas-solid flow characteristics of precalciners, respectively. Fellaou [8] used modeling to analyze the combustion efficiency of cement kiln precalciners and developed an optimization approach to reduce the total organic carbon (TOC) by 60%.

Fan [9], Bae [10], and Hu [11] studied the influence of gas components on NO_x reduction. Fu [12] studied the influence of $CaCO_3$ on the SNCR De-NO_x process and explained the mechanism of said influence. Xia [13] found that the distribution of each component was highly non-uniform in the incinerator, making the injection position of the reducing agent a very sensitive operating parameter influencing the SNCR De-NO_x efficiency. Kang [14] studied the gas-solid characteristics of cyclone separators, with the results indicating that the temperature window of the SNCR method was located in the range of 1123 K to 1323 K. Furthermore, the reduction efficiency reached a peak at 1223 K, where the normalized stoichiometric ratio (NSR) was 1.5.

Existing studies mainly focused on the characteristics of flow or the optimization of the SNCR method. Recently, Li [15] experimentally verified the adverse effect of the high CaO concentration in the precalciner on NO_x reduction. The efficiency of the traditional SNCR method can hardly be further improved for this reason.

Recently, Taniguchi found that NO_x reduction in a high temperature and fuel-rich zone was achieved on a drop-tube furnace [16, 17]. Based on his research, a new method is proposed to reduce NO_x by which ammonia is injected in the high-temperature (T>1500 K) and lean-oxygen zone (HT-DeNO_x) during pulverized coal combustion. HT-DeNO_x is significantly different from the traditional SNCR. In the paper, the feasibility of this method is verified to achieve NO_x reduction in the cement precalciner by numerical simulation.

2. Geometrical Model and Boundary Condition

2.1 Geometrical model

The outer configuration of the triple-sprayed precalciner can be divided into two cone sections and three column sections along the Z-axis. Fig. 1 shows the structure and mesh of the lowest part of the precalciner. From Fig. 1(a), it can be seen that there are four types of inlets: the gas inlet, which contains 10.1% CO_2 and 1.4% O_2 by mass; the wind inlets, which contain 23.3% O_2 and 76.7% N_2 by mass; the coal inlets, where pulverized coal is transported by air with 23.3% O_2 and 76.7% N_2 by mass; and the lower raw meal feeder, which accounts for 80% of the total raw meal mass flow. The flue gas coming from the kiln enters the precalciner vertically from the bottom. The tertiary air coming from the kiln enters the precalciner in a direction perpendicular to the wall. The four coal inlets are divided into two layers, with one half located at the lower cone of the precalciner and the other half located at the same height as the center of the lower raw meal inlet. The higher raw meal inlet is located at the middle of the precalciner, shouldering 20% of the total raw meal mass flow. All the components leave the precalciner from the top. Fig. 1(b) shows the mesh of the lowermost part of precalciner, with refined unstructured tetrahedral mesh used in all the inlets and high-quality structured hexahedral mesh used in the remaining areas. The details of the meshes are shown in Fig. 1(c).

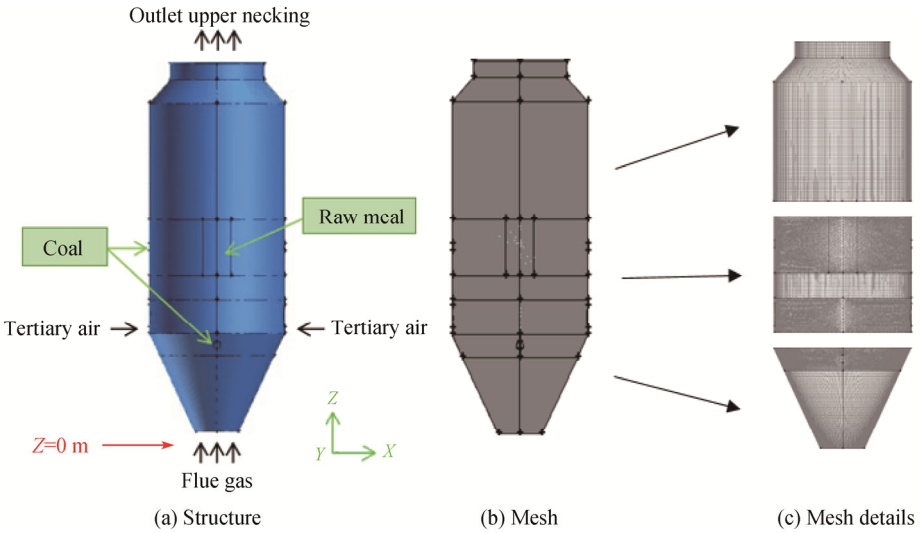

Fig. 1 Precalciner structure and mesh

2.2 Boundary condition

The operating parameters of the considered cement precalciner are listed in Table 2. The gas-phase flow was simulated by the finite volume method. The boundary conditions used in the simulation are listed below.

(1) The mass flows of tertiary air and flue gas were 25.36 kg/s and 26.7 kg/s, and the temperatures of tertiary air and flue gas were set as 1183 K and 1343 K.

(2) The mass flow was 3.52 kg/s for the pulverized coal and 54 kg/s for the raw meal, of which the main component was $CaCO_3$ (SiO_2 was ignorable for its inertia). The Rosin-Rammler distribution function was used to measure the particle diameters of both pulverized coal and raw meal. For pulverized coal, the maximum diameter was 80 μm; the minimum diameter was 20 μm, and the average diameter was 60 μm. For raw meal, the maximum diameter was 50 μm; the minimum diameter was 30 μm, and the average diameter was 40 μm.

(3) The pressure at the outlet (that is, the outlet located at the height of 50 m when compared to Z=0 m) was set to –300 Pa. The proximate analysis and calorific value are listed in Table 3; the ultimate analysis of the coal is listed in Table 4, and the raw material compositions are listed in Table 5.

Table 2 Parameters of precalciner

Parameters	Value
Model of precalciner	TTF
Production capacity	3800 t/d
Coal consumption	11 t/h
Height of precalciner	50 000 mm
Width of precalciner	5800 mm
Gas residence time	5.7 s
Average temperature at the outlet	1170 K
Injection ammonia height	42 000 mm
20% ammonia solution consumption	0.3 t/h
NO_x emission value	385 mg/m^3
Ammonia slip rate	9×10^{-6}

NO_x emission value (convert into NO_2, based on 10% O_2)

Table 3 Proximate analysis and calorific value of coal

Sample	Proximate analysis/%				$Q_{net,ar}$/MJ·kg^{-1}
	M_{ad}	A_{ad}	V_{ad}	FC_{ad}	
Coal	2.51	26.67	25.79	45.03	20.95

Table 4 Ultimate analysis of coal

Sample	Mole fraction/%				
	C_{daf}	H_{daf}	O_{daf}	N_{daf}	S_{daf}
Coal	82.00	5.03	10.57	1.28	1.12

Table 5 Raw material compositions/wt.%

Loss	SiO_2	Al_2O_3	Fe_2O_3	CaO	MgO
37.51	13.25	3.09	2.18	41.64	2.33

2.3 Mesh independence

Before the calculation, it is necessary to verify the mesh independence. The mesh totals were set as 11.72 million and 14.44 million, respectively. The two meshes were used to calculate results separately. Three independent points were selected for the comparison of the temperature values. The coordinates of the three points were Point 1 (0, 0, 10), Point 2 (0, 0, 12), and Point 3 (0, 0, 14). The results of the three points are listed in Table 6.

Table 6 Comparison of temperature values under different mesh totals

Mesh total	Point 1 (0,0,10)	Point 2 (0,0,12)	Point 3 (0,0,14)
11.72 million	1642 K	1484 K	1397 K
14.44 million	1658 K	1499 K	1411 K

As shown in Table 6, the simulated temperature differences of all three points were maintained within 20 K, which could be regarded as a stable temperature distribution. The mesh total of 11.72 million effectively simulated the thermal distribution of the precalciner and met the required accuracy. Based on the principle of the most simplified calculation, the 11.72 million mesh was selected to continue the simulation study.

3. Mathematical Model and Numerical Solution Method

3D CFD software was used to carry out the numerical simulation. An actual triple-sprayed furnace (TTF-Type) cement precalciner was simulated on a Tianhe-2A supercomputer. The pulverized coal combustion and the raw meal decomposition reactions were carried out simultaneously in the precalciner. In a previous study, we modeled the mechanisms of these reactions and found that the simulated temperature, flow rate, proportion of each material component, raw material decomposition rate, and NO_x concentration at the outlet were all highly consistent with data from the online monitoring system of a factory [18]. These results proved the credibility of the mathematical models, so the same models were chosen for the present study.

3.1 Mathematical model

The continuity equation (Eq. (1)), the momentum equation (Eq. (2)), and the energy equation (Eq. (3)) were used in the paper, shown as below.

$$\frac{\partial \rho}{\partial t}+\operatorname{div}(\rho U)=0 \tag{1}$$

$$\frac{\partial(\rho \mu_i)}{\partial t}+\operatorname{div}(\rho \mu_i U)=-\frac{\partial p}{\partial x_i}+\operatorname{div}(\mu \operatorname{grad} \mu_i)+S \tag{2}$$

where p is the static pressure; μ is the hydrodynamic viscosity; S is the source term; U is velocity; ρ is density.

$$\frac{\partial(\rho h)}{\partial t}+\frac{\partial(\rho \mu_i h)}{\partial x_i}=-p \operatorname{div} U+\operatorname{div}(\lambda \operatorname{grad} T)+\Phi+S_h \tag{3}$$

where h is the fluid ratio; λ is the thermal conductivity of the fluid; S_h is the internal heat source; Φ is the dissipative function equation of state.

3.1.1 Turbulence model

The realizable k-ε model was used in the turbulence model to solve the continuity and momentum equations in the fluid-phase [19]. In this model, k and ε are expressed as

$$\begin{aligned}\frac{\partial}{\partial t}(\rho k)+\frac{\partial}{\partial x_j}(\rho k \mu_j)=&\frac{\partial}{\partial x_j}\left[\left(\mu+\frac{\mu_t}{\sigma_k}\right)\frac{\partial k}{\partial x_j}\right]\\&+G_k+G_b-\rho\varepsilon-Y_M+S_k\end{aligned} \tag{4}$$

$$\begin{aligned}\frac{\partial}{\partial t}(\rho \varepsilon)+\frac{\partial}{\partial x_j}(\rho \varepsilon \mu_j)=&\frac{\partial}{\partial x_j}\left[\left(\mu+\frac{\mu_t}{\sigma_\varepsilon}\right)\frac{\partial \varepsilon}{\partial x_j}\right]\\&+\rho C_1 S\varepsilon-\rho C_2\frac{\varepsilon^2}{k+\sqrt{\nu\varepsilon}}\\&+C_{1\varepsilon}\frac{\varepsilon}{k}C_{3\varepsilon}G_b+S_\varepsilon\end{aligned} \tag{5}$$

where $C_1=\max\left[0.43,\frac{\eta}{\eta+5}\right]$; $\eta=S\frac{k}{\varepsilon}$; $S=\sqrt{2S_{ij}S_{ij}}$; $C_{1\varepsilon}$ and C_2 are constants; and G_k is the turbulent energy due to the mean velocity gradients.

3.1.2 Discrete phase model

The discrete phase model was used to simulate the track of pulverized coal along with the raw meal [20, 21], shown as

$$\frac{\mathrm{d}\mu_\mathrm{p}}{\mathrm{d}t}=F_\mathrm{D}(\mu-\mu_\mathrm{p})+\frac{g_\chi(\rho_\mathrm{p}-\rho)}{\rho_\mathrm{p}}+F_\chi \tag{6}$$

where μ_p is the particle velocity; μ is the fluid velocity; $F_\mathrm{D}(\mu-\mu_\mathrm{p})$ is the drag force per unit particle mass; $\frac{g_\chi(\rho_\mathrm{p}-\rho)}{\rho_\mathrm{p}}$ is the force of gravity; and F_χ represents additional forces.

The discrete random walk model was used to predict the turbulence in the gaseous phase and the stochastic tracking model was used to predict the particle dispersion due to the turbulence.

3.1.3 Chemical reaction model

The species-transport model was used to express the chemical reactions (including pulverized coal combustion and raw meal decomposition) in the precalciner [22, 23]. The coal-combustion process was assumed as volatile separation and combustion first and then the combustion of char. The volatile combustion was modeled using the two-competing-rates model.

$$C_{1.32}H_{4.15}O_{0.55}N_{0.0758}+1.42O_2 \rightarrow 1.32CO+2.075H_2O+0.0379N_2 \quad (R1)$$

The combustion of char was modeled using the first-order Arrhenius model, in which the surface reaction was used. And s in the brackets means solid.

$$C(s)+O_2 \rightarrow 0.5CO+0.5CO_2 \quad (R2)$$

$$C(s)+CO_2 \rightarrow 2CO \quad (R3)$$

$$2CO+O_2 \rightarrow 2CO_2 \quad (R4)$$

The raw meal decomposition was modeled by the Eddy-Dissipation concept model, and the surface reaction was also used to measure the reaction process.

$$CaCO_3(s) \rightarrow CaO(s)+CO_2 \quad (R5)$$

3.1.4 Radiation model

The radiation progress was modeled by the discrete ordinates model.

$$\begin{aligned}&\nabla\cdot\left[I(\vec{r},\vec{s})\vec{s}\right]+(a+\sigma_\mathrm{s})I(\vec{r},\vec{s})\\&=an\frac{\sigma T^4}{\pi}+\frac{\sigma_\mathrm{s}}{4\pi}\int_0^{4\pi}I(\vec{r},\vec{s}')\Phi(\vec{s}\cdot\vec{s}')\mathrm{d}\Omega'\end{aligned} \tag{7}$$

where $\vec{s}$ is the scattering vector; a is the absorption coefficient; n is the refractive coefficient; σ_s is the scattering coefficient; σ is the Stephen-Boltzmann constant; I is the radiation intensity; T is the temperature; and Ω' is the solid angle.

3.1.5 NO_x model and De-NO_x model

According to different formation principles, NO_x can be classified as thermal-NO_x, fuel-NO_x, and prompt-NO_x. Thermal-NO_x is not likely to be generated in the precalciner, for it is mainly formed above 1500°C while the internal temperature of the precalciner rarely rises above it. Thermal-NO_x in the precalciner was mainly transmitted from the rotary kiln. Fuel-NO_x is generated by nitrogen in the pulverized coal and is the predominant form of NO_x produced in the precalciner. Prompt-NO_x is formed in the prompt reaction of the flame front, which only accounts for a small proportion of the total NO_x, so it is negligible. The total NO_x counts as

$$S_{NO}=S_{Thermal,NO}+S_{Fuel,NO} \tag{8}$$

where $S_{Thermal,NO}$ is the reaction rate of thermal-NO_x, and $S_{Fuel,NO}$ is the reaction rate of fuel-NO_x.

The NO_x reduction occurs during the post-treatment part of the simulation process, so the SNCR model was activated on the basis of stable temperature field, velocity field, and concentration distribution of each component. The reducing agent used in the precalciner was a 20% by mass ammonia solution. The injection of ammonia

solution was modeled by the droplet model. NH_3 first volatilized from the ammonia solution and then reacted with NO. The mechanism is simplified as

$$4NH_3 + 4NO + O_2 \rightarrow 4N_2 + 6H_2O \quad (R6)$$

$$4NH_3 + 2NO_2 + O_2 \rightarrow 3N_2 + 6H_2O \quad (R7)$$

Since NO_2 only accounts for a 5% mass fraction of the total NO_x, it can be treated as NO; thus, reaction 7 is negligible.

NSR was used to measure the ratio of the reducing agent NH_3 to pollutant NO, which can be expressed as

$$\mathrm{NSR} = \frac{\text{mole fraction of } NH_3}{\text{mole fraction of NO}} \quad (9)$$

The mechanism of HT-DeNO_x is different from that of SNCR. The intermediates generated in SNCR De-NO_x reactions are [O] and [OH], which govern the rate of the reactions, and the existence of O_2 is extremely important for SNCR De-NO_x reactions. Meanwhile, the conditions required for HT-DeNO_x are high temperature (>1500 K) and fuel-rich (trace oxygen) according to the study of Taniguchi [16, 17]. Reaction 8 is suppressed, whereas the competitive reaction 9 is carried out more thoroughly. Besides, the nitrogen in pulverized coal turns into intermediate HCN first, and reaction 10 is suppressed while reaction 11 is carried out more thoroughly due to the existence of HCN. This method can further improve the reduction efficiency based on the traditional SNCR method. Since no such model was provided in the software, the simulation of HT-DeNO_x was accomplished by manually adding the reactions and corresponding parameters into the software tool. The mechanism was simplified as

$$4NH_3 + 5O_2 \rightarrow 4NO + 6H_2O \quad (R8)$$

$$4NH_3 + 6NO \rightarrow 5N_2 + 6H_2O \quad (R9)$$

$$\mathrm{HCN(intermediate)} + O_2 \rightarrow \mathrm{NO} \quad (R10)$$

$$\mathrm{HCN(intermediate)} + \mathrm{NO} \rightarrow N_2 \quad (R11)$$

3.2 Numerical solution method

To discretize the control equations of the fluid phase and solve the difference equations, the controlling-volume method and a second-order upwind difference scheme were used. To couple the pressure and velocity, the SIMPLE algorithm was used. When the convergence criterion was less than 10^{-6} for the continuity and energy term and less than 10^{-3} for the remaining residuals, the process was finished. When the convergence criterion was less than 10^{-8} for the relating equations of SNCR De-NO_x and high temperature zone NO_x reduction, the calculation was stopped in the post-treatment process.

4. Results and Discussion

4.1 Results verification

The gas composition at the outlet is displayed in Table 7. The excess air coefficient of the predicted value was based on 1.1. When unified to the measured value 1.2, the predicted value and measured value showed a high degree of coincidence. Furthermore, the predicted burnout ratio of pulverized coal was 94%, and the decomposing ratio of raw meal was 91%, both of which coincided with the data from the online monitoring system in the cement production process. The definitions of the burnout ratio of pulverized coal and the decomposing ratio of raw meal are expressed as follows:

$$\text{Burnout ratio of pulverized coal} = 1 - \frac{\text{mass flow of coal at the outlet}}{\text{initial mass flow of coal}} \quad (10)$$

$$\text{Decomposition ratio of raw meal} = \frac{100}{56} \times \frac{\text{mass flow of CaO at the outlet}}{\text{initial mass flow of } CaCO_3} \quad (11)$$

Table 7 Gas composition analysis

Mass fraction/%	CO_2	O_2	H_2O	CaO	$CaCO_3$	N_2
Predicted value (α=1.1)	28.3	0.9	1.0	24.6	4.3	40.9
Predicted value (α=1.2)	25.1	3.4	0.9	21.9	3.8	44.9
Measured value (α=1.2)	26.0	3.4	0.9	22.8	1.7	45.2

As shown in Fig. 2, the simulated NO_x concentration at the outlet after SNCR reduction was 386 mg/m^3 (converted to NO_2 and based on 10% O_2), which coincided with the NO_x emission concentration from the online monitoring system in the cement production process. Thus, the feasibility of HT-DeNO_x was studied under this operating condition.

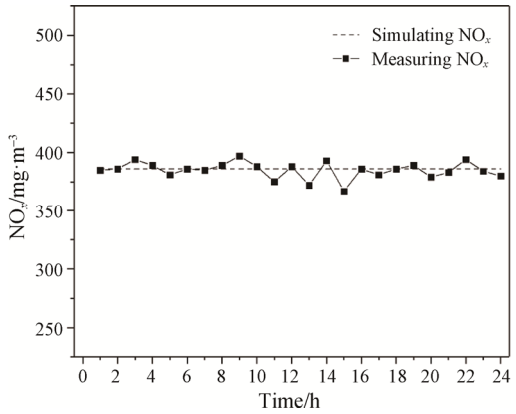

Fig. 2 Comparison of the predicted value and measured value of NO_x concentration

4.2 Influencing factors of NO_x reduction in high temperature zone

As shown in Fig. 3(a), the pulverized coal rises with the flue gas and burns in the air, releasing a large amount of heat. The heat diffuses by convective heat transfer and radiation heat transfer. Due to the effect of the boundary layer, the region near the wall is prone to heat

accumulation, which can lead to overheating. The temperature gradually decreases above the tertiary air due to the joint effect of the combustion of pulverized coal and the decomposition of the raw meal. The lowest temperature is formed in the region close to the centerline between 9.5 m and 14 m, and the height of the lowest temperature region is 3 m to 5 m above that of the lower raw meal inlet due to the ascending air flow.

In Fig. 3(b), each component shows similar axisymmetric distribution characteristics due to the axisymmetric characteristic of the precalciner. In the condition of controlling the excess air coefficient in the precalciner, the region presents a fuel-rich characteristic. The O_2 concentration is high around the pulverized coal burner inlets and the tertiary air inlets due to the input of air, but the O_2 concentration is less than 2% elsewhere. And in the region near the centerline of the precalciner, a large amount of oxygen is consumed due to the combustion of pulverized coal, so the O_2 concentration decreases gradually here. Due to the effect of the boundary layer and the reflux of the tertiary air, the O_2 concentration is less than 0.5% in the region near the lowermost necking and above the tertiary air.

Combining Fig. 3(a) and 3(b), the region between the upper pulverized coal burner and the tertiary air inlets simultaneously fulfills the requirements of high temperature (>1500 K) and fuel-rich (trace oxygen) for HT-DeNO$_x$, and the results above are achieved based on this condition.

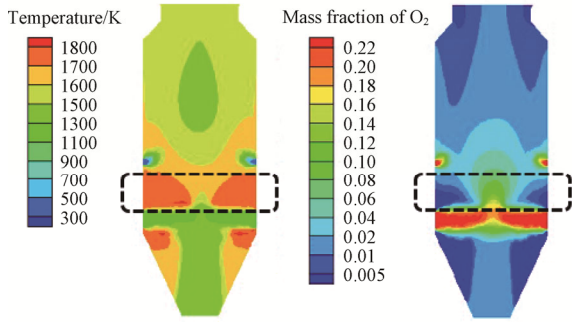

Fig. 3 Temperature field and distribution of O_2

4.3 NO_x reduction in high temperature zone

The height of 6 m in the precalciner was selected as the position of HT-DeNO$_x$, where the reducing agent was to be injected into the precalciner. The reducing agent used was a 20% ammonia (by mass fraction) solution. Six spray guns were evenly distributed in a single layer around the circumference of the precalciner, and each spray gun was perpendicular to the wall and inserted into the precalciner for a depth of 200 mm. The reducing agent particle size after atomization was 60 μm; the reducing agent injection speed after atomization was 10 m/s; the spray gun formed a conical coverage region where the semi-apex angle was 30°, and the total mass flow of the reducing agent was 0.007 kg/s, which means NSR=0.1.

In Fig. 4, the NO_x concentration is divided into four zones in the precalciner, which are high temperature zone, raw meal dilution zone, steady zone, and SNCR zone. Furthermore, the NO_x concentration in the high temperature zone is divided into five zones: three dilution zones, one formation zone, and one steady zone. In the original condition, the flue gas inlet contained a large amount of thermal-NO_x, with the concentration of about 1220×10^{-6}. The coal wind conveyed by the pulverized coal burner diluted the NO_x concentration, reducing the NO_x concentration in the region between 4 m and 5 m, and the valley NO_x concentration was formed here. At the height above 5 m, the pulverized coal was fully mixed and burned with tertiary air, the nitrogen in pulverized coal was converted into a large amount of fuel-NO_x, and the NO_x concentration increased rapidly and obtained a peak of 1253×10^{-6}. At the height >6 m, almost all the nitrogen in the pulverized coal had already converted into fuel-NO_x, so the NO_x concentration could not rise, while the tertiary air still retained a large amount of N_2, leading to a strong dilution effect on the NO_x concentration. The region between 7 m and 9 m contained the lower raw meal inlet, which also had a dilution effect on the NO_x concentration. At the height above 9 m, the NO_x concentration tended to be stable because there was no inlet. While in the reduction condition, the reducing agent was in full contact with NO due to the conical coverage. The NO_x reduction proceeded violently in the high temperature zone, making the NO_x concentration decrease rapidly: The value of the NO_x concentration peak reduced from 1253×10^{-6} to 998×10^{-6}. The NO_x reduction proceeded gently afterward, and the NO_x concentration tended to be stable, just like the tendency in the original condition. At the upper necking region of 16 m, the average cross-sectional concentration of NO reduced from 696×10^{-6} before to 503×10^{-6} after the HT-DeNO$_x$. The reduction efficiency in the high temperature zone reached 27.72% at NSR=0.1; when compared with the 50.83% NO_x reduction efficiency of SNCR at NSR=1.2, the efficiency of NO_x reduction in terms of reducing agent consumption was much higher in the high temperature zone than in the SNCR zone, which can be seen from the mechanism that Reactions (8)–(11) dominated the process of reduction, and Reactions (8) and (10) were suppressed due to the trace oxygen concentration, while competitive Reactions (9) and (11) were carried out more thoroughly. Furthermore, HT-DeNO$_x$ not only removed the NO_x that had already been generated but also converted the intermediate HCN generated by the combustion of coal into N_2 instead of NO during the reaction process, which decreased

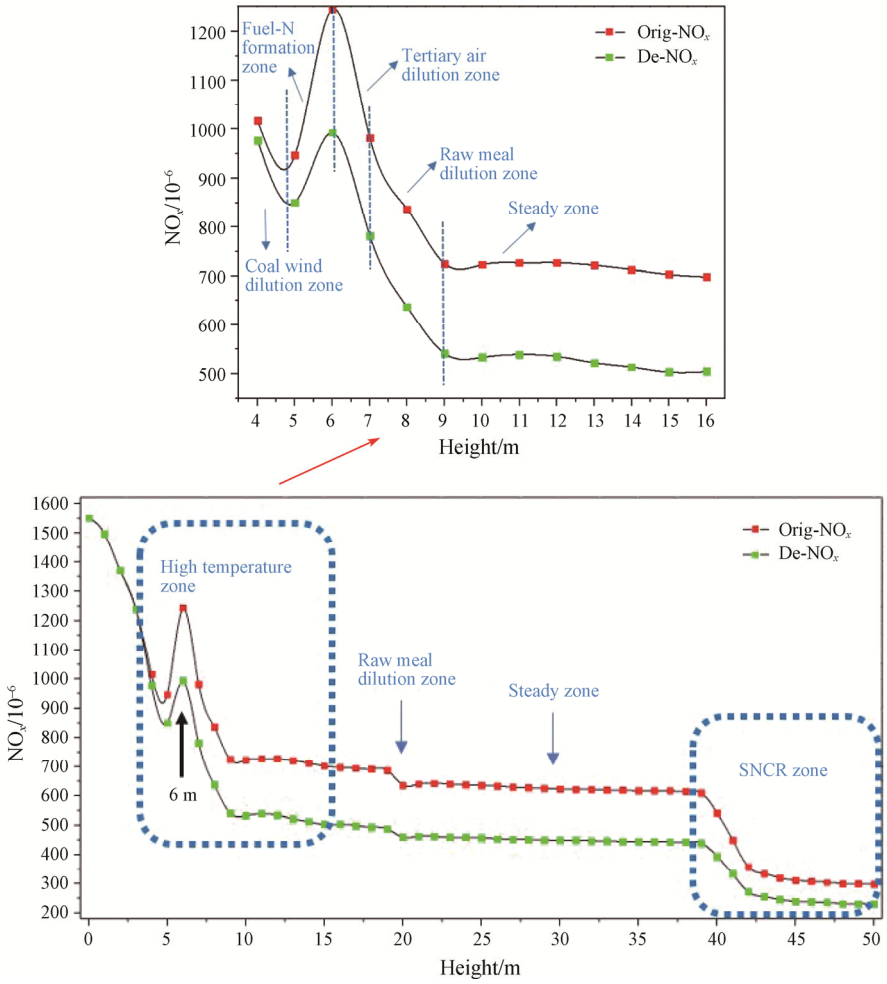

Fig. 4 Comparison of NO_x concentration before and after ammonia reduction

the amount of NO that remained. The ammonia slip rate was 9×10^{-6} at the outlet, which meets the national standard.

4.4 Different combinations and efficiency of SNCR and HT-DeNO_x

As shown in Fig. 5, the reduction efficiency of HT-DeNO_x was 27.72% at NSR=0.1. When HT-DeNO_x was combined with SNCR at NSR=1.1, the overall NO_x reduction efficiency reached 60.05% compared to 50.83% for SNCR at NSR=1.2, which means the NO_x reduction efficiency increased by 9.22 percentage points based on the same operating cost. When HT-DeNO_x at NSR=0.1 was combined with SNCR at NSR=1.2, the overall NO_x reduction efficiency was 62.64%. Thus, compared to 50.83% (the efficiency of SNCR at NSR=1.2), the NO_x reduction efficiency improved by 11.71 percentage points with an increase in operating cost of 8.33 percentage points. When compared to SNCR at NSR=1.3, the NO_x reduction efficiency still increased by 8.23 percentage points, which shows a good efficiency improvement.

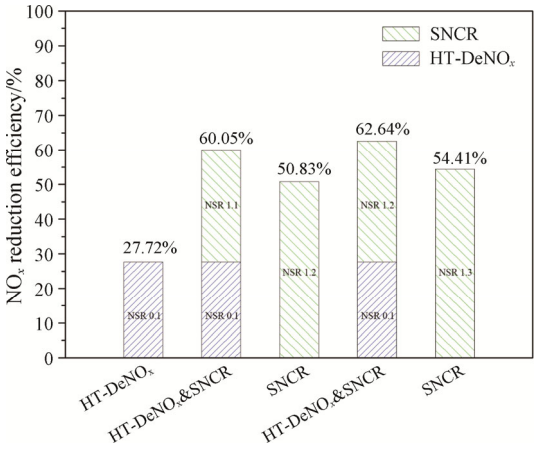

Fig. 5 Reduction efficiency under different combinations of SNCR and HT-DeNO_x

5. Conclusions

(1) An actual triple-sprayed furnace (TTF-Type) cement precalciner is simulated on a Tianhe-2A supercomputer,

and the results coincide with the actual data from the online monitoring system in the production process.

(2) The operating conditions of the HT-DeNO$_x$ zone are verified as high temperature (T>1500 K) and lean oxygen (local O_2 (in volume)<0.5%). In HT-DeNO$_x$, NO is reduced by NH_3 and HCN during the reaction process via the following reactions:

$$4NH_3 + 6NO \rightarrow 5N_2 + 6H_2O$$

$$HCN(\text{intermediate}) + NO \rightarrow N_2$$

(3) The efficiency of NO reduction by only HT-DeNO$_x$ (NSR=0.1) is 27.72%. The reduction efficiency will be improved to 60.05% and 62.64% through combining HT-DeNO$_x$ (NSR=0.1) and SNCR (NSR=1.1 and 1.2), respectively.

Acknowledgments

This work was financially supported by key Research and Development Plan of China (No.2016YFB0601503).

References

[1] Mei S., Xie J., Chen X., Numerical simulation of the complex thermal processes in a vortexing precalciner. Applied Thermal Engineering, 2017, 125: 652–661.

[2] Yan D., Peng Z., Karstensen K.H., Destruction of DDT wastes in two preheater/precalciner cement kilns in China. Science of the Total Environment, 2014, 476: 250–257.

[3] Battye R., Walsh S., Greco J.L., NO$_x$ control technologies for the cement industry (final report). EPA Contract, 2000.

[4] Hampartsoumian E., Folayan O.O., Nimmo W., Optimisation of NO$_x$ reduction in advanced coal reburning systems and the effect of coal type. Fuel, 2003, 82(4): 373–384.

[5] Maly P.M., Zamansky V.M., Ho L., Payne R., Alternative fuel advanced reburning. Washington DC, United States: Coal and Slurry Technology Association, 1997.

[6] Li X., Ma B., Hu Z., Computational modeling of aerodynamic characteristics in sprayed and spiraled precalciner. Communications in Nonlinear Science and Numerical Simulation, 2008, 13(6): 1205–1211.

[7] Liu H., Liu W., Zheng J., Ding J., Zhao X., Lu H., Numerical study of gas-solid flow in a precalciner using kinetic theory of granular flow. Chemical Engineering Journal, 2004, 102(2): 151–160.

[8] Fellaou S., Harnoune A., Seghra M.A., Bounahmidi T., Statistical modeling and optimization of the combustion efficiency in cement kiln precalciner. Energy, 2018, 155: 351–359.

[9] Fan W., Zhu T., Sun Y., Lv D., Effects of gas compositions on NO$_x$ reduction by selective non-catalytic reduction with ammonia in a simulated cement precalciner atmosphere. Chemosphere, 2014, 113: 182–187.

[10] Bae S.W., Roh S.A., Kim S.D., NO removal by reducing agents and additives in the selective non-catalytic reduction (SNCR) process. Chemosphere, 2006, 65(1): 170–175.

[11] Hu Z., Lu J., Huang L., Wang S., Numerical simulation study on gas-solid two-phase flow in pre-calciner. Communications in Nonlinear Science and Numerical Simulation, 2006, 11(3): 440–451.

[12] Fu S., Song Q., Yao Q., Study on the catalysis of $CaCO_3$ in the SNCR deNO$_x$ process for cement kilns. Chemical Engineering Journal, 2015, 262: 9–17.

[13] Xia Z., Li J., Wu T., Chen C., Zhang X., CFD simulation of MSW combustion and SNCR in a commercial incinerator. Waste Management, 2014, 34(9): 1609–1618.

[14] Kang Z., Yuan Q., Zhao L., Dai Y., Sun B., Wang T., Study of the performance, simplification and characteristics of SNCR de-NO$_x$ in large-scale cyclone separator. Applied Thermal Engineering, 2017, 123: 635–645.

[15] Li S., Ge Y., Wei X., Experiment on NO$_x$ reduction by advanced reburning in cement precalciner. Fuel, 2018, 224: 235–240.

[16] Masayuki T., Kenji Y., Hironobu K., Kenji K., A reduced NO$_x$ reaction model for pulverized coal combustion under fuel-rich conditions. Fuel, 2002, 81(3): 363–371.

[17] Masayuki T., Yuki K., Teruyuki O., Kenji Y., Hisayuki O., A role of hydrocarbon reaction for NO$_x$ formation and reduction in fuel-rich pulverized coal combustion. Combustion and Flame, 2010, 157: 1456–1466.

[18] Zhang L., Wei X., Li S., Zhai Y., Numerical simulation of O_2/CO_2 combustion in large cement precalciner. SCIENTIA SINICA Technologica, 2019, 49(9): 1080–1088. (in Chinese)

[19] Shih T.H., LiouW .W., Shabbir A., Yang Z., Zhu J., A new k-ε eddy-viscosity model for high reynolds number turbulent flows-model development and validation. Computers & Fluids, 1995, 24(3): 227–238.

[20] Rahmanian B., Safaei M.R., Kazi S.N., Ahmadi G., Oztop H.F., Vafai K., Investigation of pollutant reduction by simulation of turbulent non-premixed pulverized coal combustion. Applied Thermal Engineering, 2014, 73(1): 1222–1235.

[21] Gómez M.A., Porteiro J., de la Cuesta D., Patiño D., Míguez J.L., Numerical simulation of the combustion process of a pellet-drop-feed boiler. Fuel, 2016, 184: 987–999.

[22] Musto M., Rotondo G., CFD analysis of a realistic reduced-scale modeling equipped with axial jet fan. Fire Safety Journal, 2015, 74: 11–24.

[23] Branco J., Coelho P.J., Costa M., Experimental and numerical investigation of turbulent diffusion flames in a laboratory combustor with a slot burner. Fuel, 2016, 175: 182–190.